We are IntechOpen, the world's leading publisher of Open Access books
Built by scientists, for scientists

6,900
Open access books available

185,000
International authors and editors

200M
Downloads

154
Countries delivered to

Our authors are among the

TOP 1%
most cited scientists

12.2%
Contributors from top 500 universities

CLARIVATE ANALYTICS
BOOK CITATION INDEX
INDEXED

WEB OF SCIENCE™

Selection of our books indexed in the Book Citation Index
in Web of Science™ Core Collection (BKCI)

Interested in publishing with us?
Contact book.department@intechopen.com

Numbers displayed above are based on latest data collected.
For more information visit www.intechopen.com

Nanostructural Deformation in Brittle-Ductile Compounds and Its Application in Fabricating Ductile Nanoparticles

Babak Alinejad and Yazdan Zare

Additional information is available at the end of the chapter

Abstract

The ball-milling process involves both fracturing and welding of particles. Particles of ductile materials are very likely to attach to each other when entrapped between balls. Therefore, conventional milling methods fail to grind ductile materials into nanoparticles. However, using brittle particles together with the starting materials, one can fracture and highly activate ductile particles through planetary ball milling. During the milling process, brittle particles are easily fractured down, and their sharp edges chop the particles of the ductile materials incessantly into pieces until both ductile and brittle particles are nano-sized (a process which is unlikely, if not impossible, to accomplish by ball milling of ductile materials alone). In this chapter, the effects of ball milling of ductile materials (e.g., graphite, aluminum, and zinc) together with a brittle material (here, NaCl), for preparation of metal nanoparticles or metal oxide nanoparticles are investigated. A theoretical explanation of the mechanism is also presented based on the facts and practical measurements.

Keywords: ball milling, brittle, ductile, nanoparticle, nanochopper, graphene

1. Introduction

In every branch of material engineering, it happens very frequently that a bulk material is ground into very fine particles. Therefore, material engineers are quite acquainted with grinding process. Having basic principles in common, grinding methods may be slightly different depending on the characteristics of the material that is about to be ground, ultimate size of particles after grinding, energy- and time-consumption condensations (which may also be referred to as economy of the process), etc.

One of the most routine methods for grinding is planetary ball milling in which a given material is loaded in a jar that is partially filled with balls made of a harder material (e.g., stainless steel and zirconia). The jar is then sealed and rotates multi-directionally by means of electromotors. The bulk material is gradually ground as the balls exert large enough compressive and shear stresses on it to fracture it into fine particles. For most of the materials, the longer the ball-milling duration, the smaller the particle size. However, as we will see soon in this chapter, this is not always the case. Particles of ductile materials rejoin together to form larger particles when they are shoved into each other by the balls (this phenomenon is referred to as *cold-welding*). Hence, the ball milling does not necessarily lead to size reduction of the particles.

Introduced in this chapter is a new, simple method for ball milling of ductile materials (the method has already been examined for some ductile materials). When the materials to be ground are all ductile, then a brittle material should be added to the jar to serve as a chopper and prevent from cold-welding of the ductile materials. Using this method, one can obtain nanoparticles of ductile materials by ball milling [1–5]. The brittle choppers also undergo size reduction down to nano size during the ball milling. Thus, they are referred to as nanochoppers in this chapter.

Along with their brittle nature, the nanochoppers should also meet some other requirements. They, for example, must not react with the starting materials. They should be harder than the starting materials, nontoxic, abundant, and economic. However, nanochoppers must have another characteristic which is of great importance: they must be easy to remove from the product, leaving no vestige.

Consequently, the overall process of obtaining nano-sized powders of ductile materials consists of two steps. The first step is ball milling of the starting materials together with a brittle material, and the second step is removal of the brittle material from the product. The latter step, however, may be accomplished by different techniques depending on the characteristics of the brittle material and ultimate objective of producing the powder. The next three sections of this chapter consider the method according to the final purpose of the ball milling: production of metal nanoparticles, production of hydrogen by means of metal nanoparticles, and production of metal oxide nanoparticles.

2. Mass production of nanoparticles of ductile materials

When one's final objective is to produce nanoparticles of a ductile metal, conventional ball-milling procedure may not come in handy as it fails to downscale the ductile metal particles. At the beginning of ball-milling process, the bulk material is fractured into smaller pieces under the pressure of the balls. However, the rate of size reduction of particles decreases as the time passes and eventually approaches to zero [6]. That is, the further ball milling does not lead to smaller particles because the rate of fracture is very low and is almost equal to the rate of cold-welding. There are several reasons for low rate of size reduction after long time. Firstly, fine particles are very unlikely to be entrapped between two balls, and if they are, the stresses exerted from the balls do not break them into pieces. Instead, the ductile particles are

only kneaded and deformed or are thrusted into each other to make a larger particle. Also, the intersection of the balls is too large (compared to the size of the particles) to rip the particles apart. When the balls are rolling against each other, they buffet the particles about, making them more susceptible to agglomerate. Under such circumstances, one should add balls with radii comparable to the size of the particles. In practice, particles of a harder, brittle material can play the role of the tiny balls. If a brittle material is added to the jar at the beginning of the ball-milling process, then it is also ground into smaller pieces, and after adequately long time, the brittle particles are nano-sized and act as nanochoppers. These nanochoppers cut the ductile particles into pieces and reduce their sizes.

Some practical instances of application of this method are introduced here. First, we show how to prepare graphene nanoflakes, and then we report the experiment conducted to extend the methodology to mass production of aluminum nanoparticles.

2.1. Preparing graphene nanoflakes

Graphene has a two-dimensional, hexagonal lattice that is composed of sp2-bonded carbon atoms [1, 7, 8]. It was first invented through micromechanical cleavage of graphite in 2004 [9], and its extraordinary characteristics [10, 11] have drawn the scientists' and engineers' attentions toward its promising applications in different fields such as composite materials, transparent conductive films, ultrasensitive gas sensors, and solar cells [12–14]. Various methods for producing graphene flakes have so far been invented which are commonly categorized into two groups: bottom-up and top-down methods. In bottom-up methods, the hexagonal carbon structure is formed from molecular precursors (e.g., epitaxial growth of graphene on substrates) [15, 16] and thermal decomposition of SiC [17]. These production processes, however, are very energy-consuming, and their yield is low. They also need expensive equipment. In the methods classified as top-down group, on the other hand, graphene layers are peeled out or extracted off the graphitic microstructures such as carbon nanotubes, carbon fibers, and graphite (or graphite oxide) by chemical, electrochemical, or physical techniques [18–20]. These techniques typically include complicated syntheses, harsh oxidizers [21], or immoderate utilization of organic solvents for exfoliation [22–24]. To produce graphene flakes in larger quantities, one may also choose mechanical milling method because it is relatively convenient and economic. However, if graphite powder is solely ground in a planetary ball mill, then the milling process augments the stress in the graphite structure [25–27]. Wet environments, on the other hand, degrade the quality of the product because liquid solution in the jar may react with the balls and the jar leaves some impurities in the product [28]. Nevertheless, as explained above, there is a convenient method for reducing the size of graphite particles incessantly by addition of a brittle material to the planetary ball mill. Owing to its convenience and low cost of involved materials, this approach can be easily scaled up.

Sodium chloride (NaCl) is used as the brittle material for ball milling of natural graphite powder. NaCl is added directly to the jar with graphite and ball milled for 2–5 h. The ball-milling process specifications are listed in **Table 1**. The resultant powder is then leached with copious amount of water in ultrasonic bath and then dried at 80°C under vacuum.

NaCl to graphite molar ratio	3
Ball-to-powder weight ratio	20
Rotational speed of the planetary ball mill	350 rpm
Atmosphere	Argon
Atmosphere pressure	0.4 MPa
Ball-milling duration	2–5 h

Table 1. Ball-milling specification for preparing graphene nanoflakes.

The structural and morphological characteristics of a powder milled under abovementioned condition are reported to be as follow:

Figure 1 demonstrates the XRD pattern of the graphite powder milled together with NaCl (the salt is removed by water). The diffraction peak (002) at $2\theta = 26°$ corresponds to a d-spacing of 0.34 nm that approximately matches the graphite (JCPDS No. 75–1621). The width broadening of the peak may be attributed to the lattice strain and size reduction of the particles.

TEM image of the produced graphene is shown in **Figure 2**. One may easily recognize the distinct layers of graphene (with approximate size of $200 \times 50 \text{ nm}^2$). As seen in the figure, the graphene flakes have ragged edges which are cut off by brittle salt particles.

Figure 3 shows the topology of the graphene powder obtained by AFM that, consistent with TEM image, confirms the ragged edges of the graphene layers.

Specific surface area of the graphene flakes produced by brittle-ductile milling technique is reported to be 524.4 m^2/g. This value is close to that of the graphene nanoflakes obtained using chemicals and microwave radiation, as reported by Sridhar et al. [29].
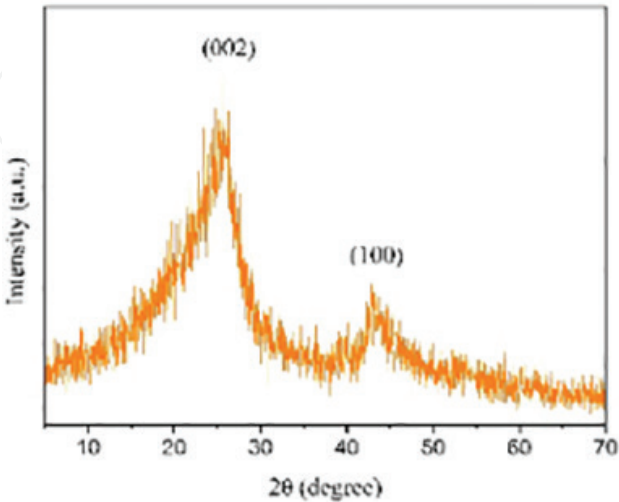

Figure 1. XRD pattern of graphite powder that is milled together with salt (salt is then washed away by water). Source: Ref. [1], Copyright @ 2017 Word Scientific.
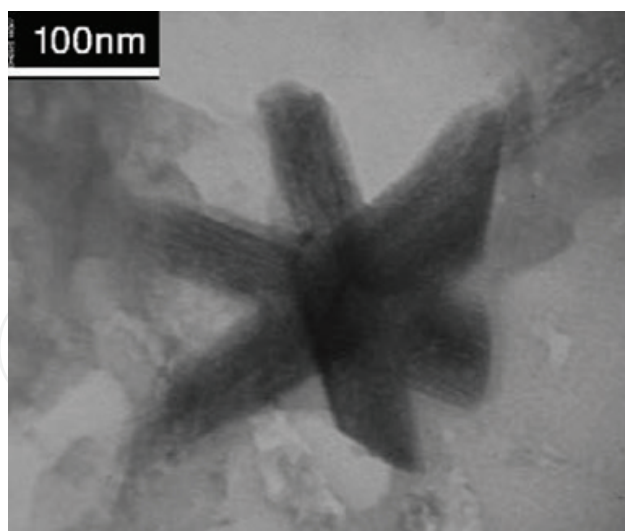
Figure 2. TEM image of graphene powder after 2 hours of milling with NaCl (salt is removed by water). Source: Ref. [1], Copyright @ 2017 Word Scientific.
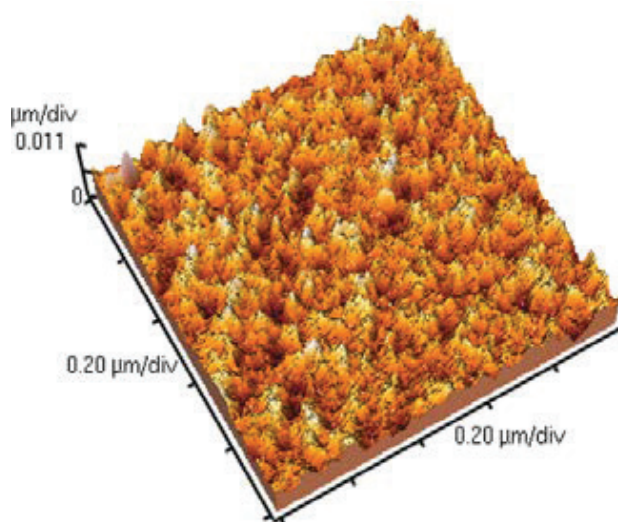

Figure 3. AFM image of the graphene flake. Source: Ref. [1], Copyright @ 2017 Word Scientific.

The average size of the particles reduces from 200 to 400 nm to about 50–150 nm as the ball-milling duration increases from 2 to 5 h. Size of salt particles also decreases during the ball milling [2] as shown in **Figure 4**. Average size of salt particles is reported to be about 150 nm after 5 h of ball milling. Owing to their brittle nature, salt particles fracture and take sharp edges by which they can cut graphite particles into smaller pieces. High salt-to-graphite molar ratio (3,1), on the other hand, retards the agglomeration of graphene flakes.

Moreover, graphene layers are exfoliated due to the sheer stress caused by random multiaxial collision of the balls which is also assisted by salt particles. Because of the random nature of the collisions and the random shape and position of the salt particles, they may exert either compressive forces that chop the graphene particles into smaller pieces or shear forces that exfoliate the layers (**Figure 5**).
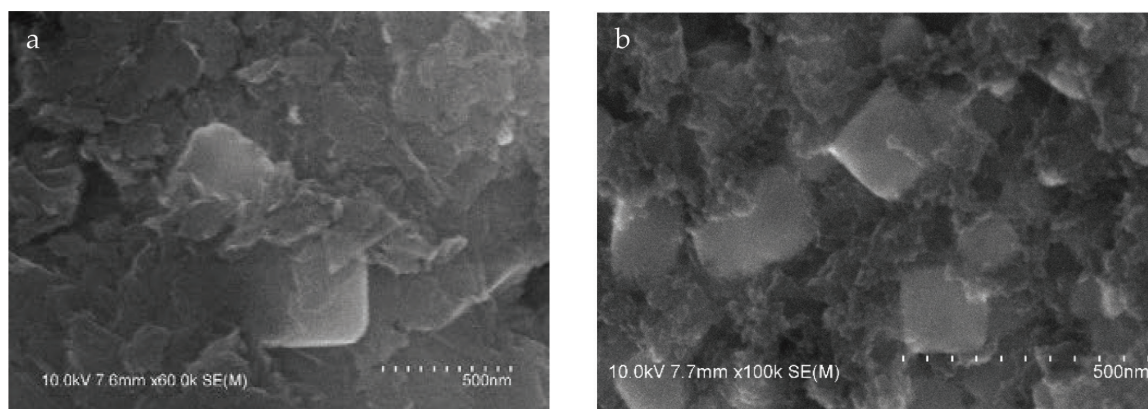
Figure 4. SEM images of graphite powder that is milled together with salt for (a) 2 h and (b) 5 h [1]. Source: Ref. [1], Copyright @ 2017 Word Scientific.

Figure 5. Exfoliation and fragmentation of graphene. Source: Ref. [1], Copyright @ 2017 Word Scientific.

As a nanochopper, salt meets almost all the requirements: it is not expensive, nor toxic; it is abundant and can be easily recycled; and, above all, it conveniently leaches out to water. Hence, this method can be employed for mass production of graphene nanoflakes because it is simple, eco-friendly, and economic.

2.2. Preparing nanoparticles of aluminum

The popularity and importance of aluminum nanoparticle are well understood by knowing its wide application in propellants and pyrotechnics. The methods of manufacturing aluminum nanoparticle are generally classified into two categories: methods involving vapor phase condensation and liquid phase chemistry. One of the vapor phase condensation methods is exploding electronically heated wires [30]. Aluminum nanoparticles, for example, are produced by condensing aluminum vapor generated by passing a strong electrical current through a thin aluminum wire. Some other techniques are occasionally used to prepare metal vapor, namely, radiative heaters, induction heaters or plasma, lasers, and electric arcs. All these techniques require a neutralized gaseous environment whose pressure strongly affects size distribution of resultant nanoparticles. At low pressures, condensation leads to formation of nano-scaled particles. The higher the pressure, the larger the particles. On the other hand, increasing the pressure increases the yield [31]. The effects of other experimental parameters, such as gaseous environment and electric pulse characteristics, are elaborately reported in [31].

All abovementioned techniques suffer from some disadvantages. Production rate is generally low in all of them. Moreover, distribution of particles size extends over a broad range from 10 nm to microns depending on the energy given to the metal. The higher the energy, the wider the distribution. On the other hand, higher energy is required for increasing the yield. This implies that there is a trade-off between the yield and size uniformity. Of course, a narrower range (i.e., uniform distribution of the particle sizes) is generally preferred.

Variations of the bulk aluminum heating technique are reported in [32] in which aluminum is ablated by an Nd-YAG laser.

The other methods of metal nanoparticle production (commonly referred to as liquid phase chemistry) are more chemical. Like all other liquid phase chemistry techniques, measured amount of starting solutions are mixed and stirred slowly, and then the product is dried. As the process is time-consuming, the methods are not appropriate for mass production. In practice, the methods require essential modifications to be qualified enough for producing nanoparticles in large quantities.

Inspired from the method introduced above for preparing graphene nanoflakes, we conducted series of experiments for preparing aluminum nanoparticles. Again, salt was used as the brittle material to serve as nanochopper. Following is the report of the experiments:

Elemental Al powder (99% purity, particle size <100 μm, Fluka) and NaCl (100–200 μm) were ground in a planetary ball mill. The jar of the ball mill was a 125 mL stainless-steel jar with radius of 15 cm. **Table 2** summarizes the specifications of the ball-milling process. The salt-to-aluminum molar ratio (hereafter denoted by η) was 2. To compare the effect of salt particles on size reduction of aluminum particles, the experiment was repeated without salt ($\eta = 0$).

After the milling process accomplished, the salt particles were washed away by immersing the powders in pure water. To prevent aluminum from reacting with water, the process of salt removal was performed using cold water at 1°C and as fast as possible. Resultant aluminum powders were characterized by scanning electron microscopy (SEM, Cambridge S 360) and X-ray diffraction (XRD, Philips 3710 W X-ray diffractometer with CuK α, $\lambda = 1.54184$ Å). The specific surface area of the powders was determined by means of nitrogen adsorption using Brunauer-Emmett-Teller method (BET-N$_2$ Micrometrics Gemini 2375).

As demonstrated in **Figure 6a**, ball-milling aluminum without salt ($\eta = 0$) has eventually reduced the size of particles to 10 μm. However, the morphology of particles is laminar and

NaCl to aluminum molar ratio (η)	0 and 2
Ball-to-powder-weight ratio	10
Rotational speed of the planetary ball mill	270 rpm
Atmosphere	Argon
Atmosphere pressure	0.4 MPa
Ball-milling duration	20 h

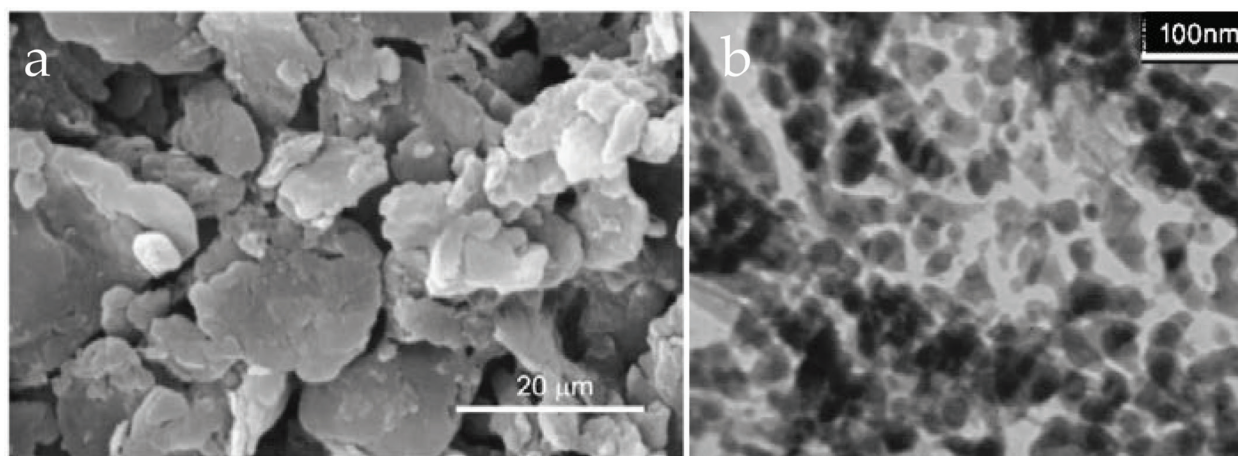**Table 2.** Ball-milling specification for preparing aluminum nanoparticles.

Figure 6. TEM image of ball-milled aluminum particles without (a) and with (b) salt, after removing the salt particles by cold water. Source: Reprinted from Ref. [5], Copyright 2009, with permission from Elsevier.

wrinkled. To reduce the size of the particles, aluminum was milled with high molar ratio of salt ($\eta = 2$). This helps aluminum particles to reach smaller sizes. Salt particles have sharp edges and are hard enough to chop aluminum particles. Due to their brittle nature, they fracture and break into smaller particles during the milling process and cut aluminum particles. Meantime, because of high η, there is a little chance for aluminum particles to meet and cold-weld. **Figure 6b** shows the micrograph of aluminum powder milled together with salt. The size of aluminum particles is decreased to less than 50 nm. Specific surface area of the powder is about 40.9 m^2/g.

Aluminum particles prepared by other methods have a hard aluminum oxide crust, while this method leads to nanoparticles with a soft aluminum hydroxide crust which is expected to show better mechanical, consolidation, and sintering behavior. Furthermore, nanoparticles produced by this method have higher lattice residual strain (cf. Section 3 of this chapter). Consequently, the aluminum nanoparticles are more active because mechanical milling causes various defects (dislocations, vacancies, grain boundaries, etc.) in them.

3. Production of hydrogen using metal nanoparticles

Environmental pollutions are one of the most serious challenges during the recent decades, and fossil fuels have the most contribution in the crisis [2]. On the other hand, fossil fuels are not renewable and will run out sooner or later. Consequently, the energy crisis has drawn scientists' attention to eco-friendly and recyclable fuels. One of the best candidates is hydrogen which is currently produced through various methods such as biological [33], water electrolysis [34], and chemical methods [35]. These methods suffer from some disadvantages: they are costly, they have typically low efficiency, and they consume fossil fuels which are neither clean nor recyclable [36, 37].

Another challenge with hydrogen as a fuel is its storage. Since the volumetric density of hydrogen is low, it needs very large storages (at 700 bars, volume of storage required for hydrogen is

about six times that for gasoline with the same energy content). The ignition energy of hydrogen, on the other hand, is 0.03 mJ, implying that it is extremely flammable [38], a fact that must be considered in designing hydrogen storage. Thus, it sounds quite reasonable idea to eliminate the need for the storage by producing hydrogen on demand. There are some hydrogen resources in the nature from which hydrogen may be extracted through a chemical process. Among all, water is the best candidate because its hydrogen content is relatively high (111 kg/m^3), it is abundant in nature, it is not costly, and it can be recycled by hydrogen combustion.

The chemical reaction through which hydrogen is obtained from water is simple: oxidation of the active metals. The only challenge is to find proper metal. According to Kravchenko et al., aluminum is the most eligible metal [39], because it is recyclable, it is the most abundant metal in the earth's crust, and its density is very low compared to other metals. The chemical reaction between aluminum and water is as follows:

$$Al + 2H_2O \rightarrow AlOOH + {}^3/_2 H_2 \qquad (1)$$
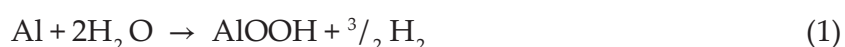
As seen, the byproduct of the reaction is aluminum oxide hydroxide which is eco-friendly and has many applications (e.g., water conditioning, papermaking, alumina production, fire prevention, and so on).

In normal condition, however, reaction (1) cannot proceed because there is a passive layer of aluminum oxide over the aluminum particles, preventing the inner aluminum atoms from reaction with water. Some solutions to the problem has been so far proposed, each of which having its own disadvantages. Immersing the aluminum in NaOH, for instance, removes the aluminum oxide layer; but it is intensely corrosive and may corrode the instruments [40–42]. Amalgamation of aluminum is another suggestion, but it involves dampening of aluminum surface with eutectic gallium-indium or mercury which are toxic and/or costly [43].

Another method for continuous hydrogen generation from aluminum is using aluminum powder with adequately small particles. This implies higher specific surface area of the powder and, consequently, more activity of the aluminum powder [44, 45]. As explained in the previous section, ordinary ball milling is unable to reduce the size of aluminum particles down to nano size because aluminum is a ductile metal. Even milling the aluminum particles together with brittle hydrides and salts (e.g., $MgCl_2$, KCl, NaCl, CaH_2, and MgH_2) with brittle-to-ductile molar ratios less than 0.1 has reportedly failed to decrease the size of the aluminum particles [46]. Also, grinding aluminum metallic composites (e.g., aluminum-bismuth) together with inorganic salts only leads to galvanic corrosion and ionic conductivity. This method provides the energy required for the reaction by the heat emerged from exothermic solution of salt. In spite the fact that the method is efficient in energy consumption, it is still ineffective in particle size reduction [46, 47], and moreover, the involved materials are costly, corrosive, and toxic.

As described in the previous section for preparing the aluminum nanoparticles, NaCl is added to the ball mill to serve as nanochopper because it is accessible, economic, easily soluble in water, nontoxic, and eco-friendly. However, η should be much higher than the reported values. Higher η (up to 15 times those reported in [46]) not only reduced the size of the aluminum particles but also increases defects in aluminum crystal by embedding salt gates [2].

As a result, specific surface area of the powder increases drastically, and reaction (1) can proceed until all aluminum content is consumed.

Since the method is simple and involves accessible materials (aluminum, salt, and water), it may be conveniently used for on-demand hydrogen generation:

For generating hydrogen from aluminum nanoparticles, one may start from elemental Al powder and ordinary salt, NaCl (100–200 μm). The mixture of aluminum and salt should be ball milled for 20 h. Ball-milling specifications are summarized in **Table 3**. The η may be selected to be as low as 0.2, but higher η leads to better result. After the milling process, about 150 mL water at a temperature of 70°C is added to the jar. Hydrogen is then released that should be condensed and dried for designated usage.

Figure 7 shows the yield of the reaction (1) as a function of time elapsed after adding water to the jar for different η's. As one may see in the figure, the efficiency of the samples with more

NaCl to aluminum molar ratio (η)	0.1, 0.2, 0.5, 1.0, and 1.5
Ball-to-powder weight ratio	20
Rotational speed of the planetary ball mill	270 rpm
Atmosphere	Argon
Atmosphere pressure	0.4 MPa

Table 3. Ball-milling specification for preparing aluminum nanoparticles for hydrogen generation.
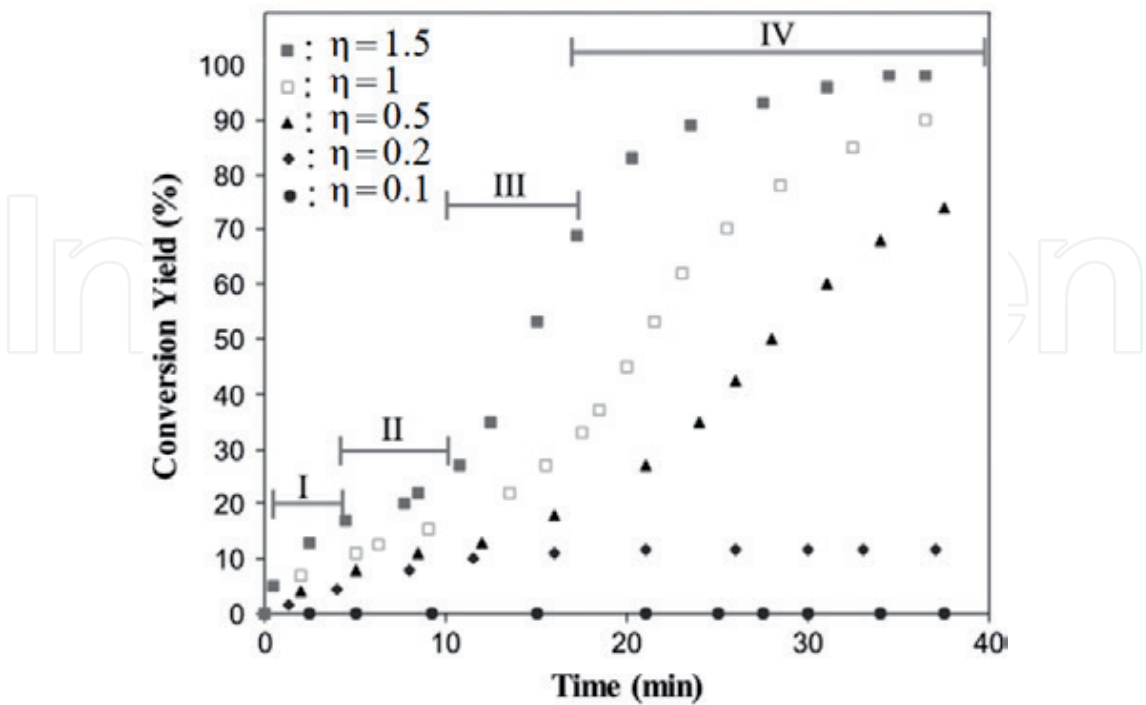

Figure 7. Conversion yield as a function of reaction time for samples with different η. Source: Reprinted from Ref. [2], Copyright 2009, with permission from Elsevier.

salt content is higher. The reaction time may be divided into four regions: In the first region, about the first 5 minutes of milling, hydrogen is mainly generated from the hydration of fresh surfaces. The higher the η in this region, the faster the reaction. This is mainly because smaller particles imply higher specific surface area. The reaction slows down as the passive AlOOH layer is formed over the surface of the particles (region II). The reaction accelerates again in region III when the salt gates dissolve, exposing fresh aluminum to water and letting water to penetrate to the core of the particles. The higher the η, the more surface of fresh aluminum and, hence, the more hydrogen generation. When all the fresh surfaces undergo the reaction, the passive AlOOH layer will eventually hinder the reaction (region IV). Almost all the aluminum atoms in the sample ball milled with η = 1.5 have undergone the reaction, while ball milling with η = 0.1 has no considerable effect on the yield. The highest rate of hydrogen generation happens in region III of the sample with η = 1.5 (75 mL/min per 1 gr of Al).

Unlike other methods (based on hydrogen generation using aluminum in which hydrogen generation is stopped when aluminum particles are covered by a layer of aluminum oxide), all the aluminum contents react with water when the particles are adequately small.

Continuous hydrogen generation may be explained as follows: Salt particles cut the aluminum particles and form local gates on the newly exposed surfaces. They also fracture into smaller particles during the ball milling due to their brittle nature. Salt particles have sharp edges and are harder than aluminum particles. During the ball milling, they rip through aluminum particles making local gates in them. When the salt particles are washed away, fresh surfaces are exposed to water.

Figure 8 is a SEM image of a salt particle among the aluminum particles for a sample with η = 0.5. Adding more salt to the jar in ball milling (i.e., higher η), of course, leads to development of more salt gates. Thus, higher η rises the kinetics of hydrolysis reaction by increasing the specific surface area of the aluminum particles in two ways: reducing the size of aluminum particles and developing salt gates in them.
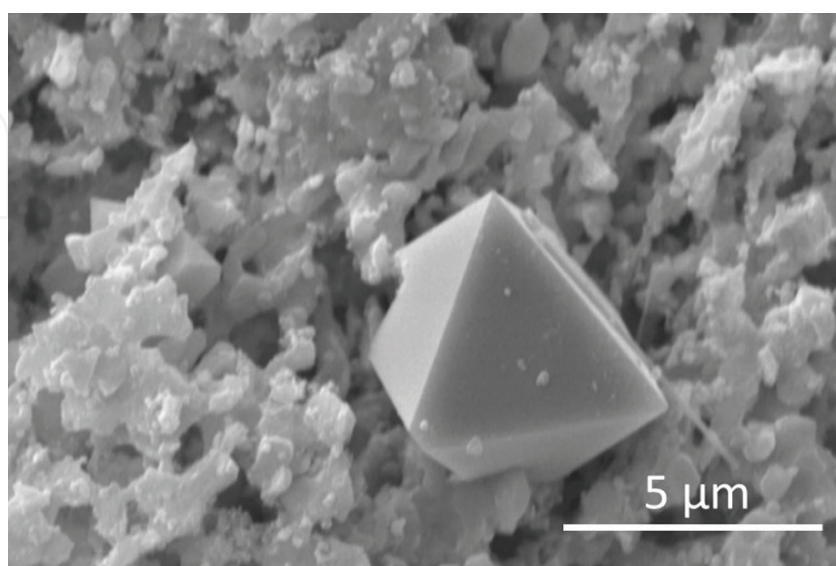

Figure 8. Salt nanochoppers in the context of aluminum nanoparticles. Source: Reprinted from Ref. [2], Copyright 2009, with permission from Elsevier.

It is worth mentioning that there are, of course, some inhibitors (e.g., stearic acid) that are assumed to prevent cold-wedding. However, they evaporate during the ball-milling process which relatively takes a long time. Therefore, they do not practically avoid the cold-welding in long-time ball milling. Furthermore, since the inhibitors are greasy, they prevent aluminum particle from reacting with water. Using salt brittle particles (with $\eta > 1.5$), one can obtain aluminum powder with particle size of about 50 nm and specific surface area of 40.9 m^2/g. This means that water can reach to the core of the particles and the reaction can proceed to release their innermost hydrogen contents. Moreover, mechanical milling gives rise to various defects in aluminum particles such as vacancies, dislocations, grain boundaries, etc.

Table 4 summarizes the lattice strain and crystallite size of the powders. The values are calculated by line broadening of XRD peaks and Williamson-Hall technique. This table suggests that adding salt to the ball mill increases the lattice strain, the fact that is also supported by XRD patterns of the samples milled with and without salt. **Figure 9** shows the XRD pattern of the samples ball milled with $\eta = 0$ (no salt) and $\eta = 1.5$. The inset in this figure magnifies the

η	Crystal structure (Å)	Crystalline size (nm)	Lattice strain (%)
0.0 (no salt)	Cubic (a = 4.046(2))	42.22(1)	0.61(4)
1.5	Cubic (a = 4.44(3))	43.13(3)	0.50(1)

Source: Reprinted from Ref. [2], Copyright 2009, with permission from Elsevier.

Table 4. Crystalline characteristics of aluminum powders milled with $\eta = 0$ (no salt) and $\eta = 1.5$.
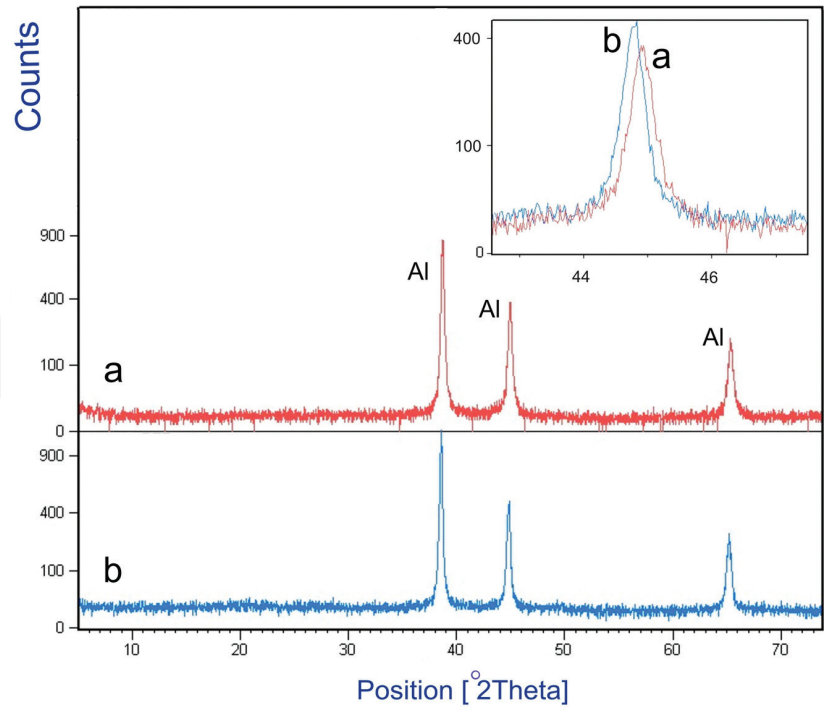

Figure 9. XRD pattern of the samples ball milled with $\eta = 1.5$ (a) and $\eta = 0$ (no salt) (b). The inset magnifies the shift of (200) peaks in the samples. Source: Reprinted from Ref. [2], Copyright 2009, with permission from Elsevier.
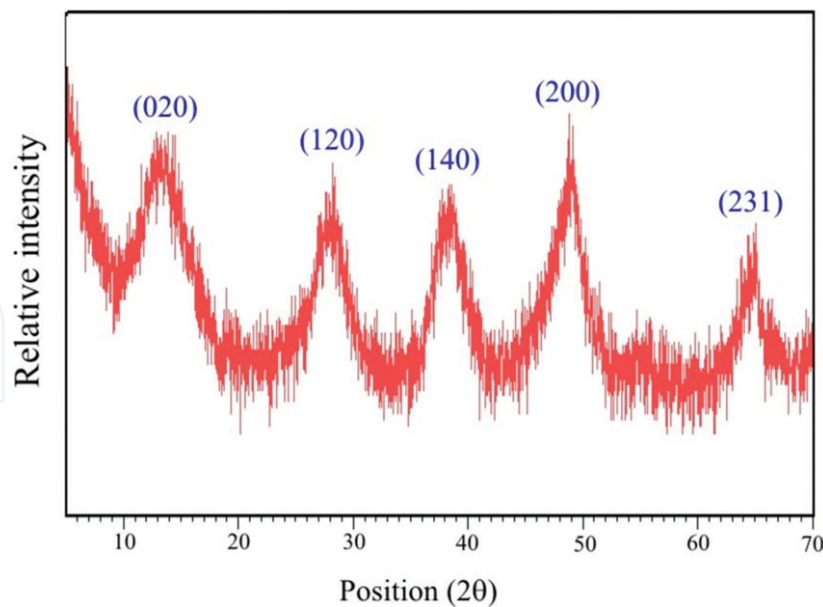
Figure 10. XRD pattern of the sample ball milled with $\eta = 1.5$ after reacting with hot water. The peaks correspond to AlOOH, and there is no evidence of aluminum. Source: Reprinted from Ref. [2], Copyright 2009, with permission from Elsevier.

XRD differences of the two samples. The lattice strain developed by ball milling provides a driving force that results in more corrosion or oxidation [14].

On the other hand, aluminum-water reaction is exothermic which helps the reaction proceed spontaneously. During hydrolysis, water temperature increases from 70°C to maximum of 74°C. Release of hydrogen in the interface of aluminum and aluminum hydroxide gel increases the porosity, letting water penetrate deep inside the aluminum particle and react with innermost atoms. X-ray diffraction pattern of the powder milled with $\eta = 1.5$ after reacting with hot water is shown in **Figure 10**, which is in good agreement with the characteristic spectrum of AlOOH crystal in the JCPDS database, except for the broader peaks due to a lower crystallinity. Aluminum is absent in the diffraction pattern, implying that reaction has reached the core of aluminum particles and entire aluminum powder has turned into AlOOH.

4. Production of metal oxide nanoparticles

The same method as explained above may be employed to prepare nanoparticles of ductile metal oxides. To examine the method for a different ductile metal, we selected a metal that its oxide is of great importance and has many applications: zinc oxide.

Even in its bulk state, zinc oxide has interesting properties: it is electrically stable with a direct band gap of 3.37 eV; it is transparent for visible light; it is abundant and nontoxic. Owing to its fabulous properties, it is widely used in various field of industry such as sensors, optoelectronic devices, solar cells, catalysts, field emission, data storage, etc. [48, 49]. On the other hand, due to its hexagonal Wurtzite structure and polar crystal surfaces, zinc oxide can take

on different nanostructures (e.g., nanorods, nanotubes, nanobelts, and nanosheets) only by restraining certain direction(s) from growing [50, 51]. The methods by which one can produce the different nanostructures are generally categorized into two groups: vapor phase process and solution phase route. The first group consists of physical vapor of the deposition, vapor phase transport and some other methods [52]. All these methods, however, have some disadvantages in common. They, for instance, require high temperatures to accomplish. Also, they need costly equipment and accomplish only when some strict conditions are all met. They sometimes employ metal catalysts (e.g., gold) to control the growth process [53]. Solution phase route group (including sol-gel and hydrothermal methods [54]) suffer from some disadvantages too: they are time-consuming and require costly chemicals. They also employ some toxic, dangerous and expensive organic solvents amine in solvothermal process.

The simplest method for producing zinc oxide is the direct reaction between zinc and water. However, as with aluminum, a thin layer of zinc oxide is formed all over the zinc particle, preventing from the reaction. Although some techniques have been proposed so far, none can synthesize zinc oxide incessantly. Using zinc foil as a substrate for growing zinc oxide, for instance, leads to formation of a thin layer of zinc oxide [55]. Another suggested method is oxidation of zinc nanoparticles. If average radius of particles is smaller than thickness of the zinc oxide layer (about 10 nm), then this method works; otherwise, the particle is coated with a zinc oxide layer hindering the core of particle from oxidation [56].

In our experiment, we tried to reduce the size of the particles (or, in other words, activate them). The activation may be performed by milling zinc powder with high molar fraction of salt (as described in previous sections). This not only reduces the size of zinc particles but also covers newly produced surfaces with salt particles that otherwise would be covered by zinc oxide layer. So, the product can be stored in the air needing no neutral gas. When the salt is leached, fresh surfaces of zinc are exposed to water. Then, all nanoparticles react with water, entirely. Instead of using zinc salts (e.g., $Zn(CH_3COO)_2.2H_2O$) and other chemicals (e.g., NaOH, KOH, etc.) or alcohol solutions (that are employed in preparing some metal oxides), only zinc, salt and water are utilized in this method. This method is highly efficient and eco-friendly and does not need costly, complex equipment. It can be employed to manufacture other metal oxide systems [5] and scaled up for mass production.

Following is the report of experiment:

Zn powder (99% purity, Mesh-325, Merck Art.No. 1.08789) and salt (100-200 μm) were ground in a planetary ball mill with the specification tabulated in **Table 5**. The ground powder was poured in 250 mL of water at 75°C and was stirred by a magnetic stirring machine at constant temperature for 5 h. The powder was then washed before being dried in an oven at 80°C and before being characterized by X-Ray Diffraction (XRD, using Philips 3710W X-Ray diffractometer with CuKα (λ = 1.54184 A°) radiation), Scanning Electron Microscopy (SEM, using Cambridge S 360) and Transmission Electron Microscopy (TEM, using Philips EM 208S). Specific surface area of the powder was determined through nitrogen adsorption by Brunauer-Emmett-Teller method (BET-N$_2$ adsorption, Micromeritics Gemini 2375).

Figure 11 shows X-ray diffraction profile of resultant zinc oxide powder. The peaks corresponding to hexagonal phase of ZnO (JCPDS 36-1451) are illustrated. Sharp peaks signify good crystallinity of zinc oxide powder. Lattice constants (a = 3.2543(1) Å and c = 5.2134(2) Å)

NaCl to zinc molar ratio	5
Ball-to-powder weight ratio	30
Rotational speed of the planetary ball mill	300 rpm
Atmosphere	Argon
Atmosphere pressure	0.4 MPa

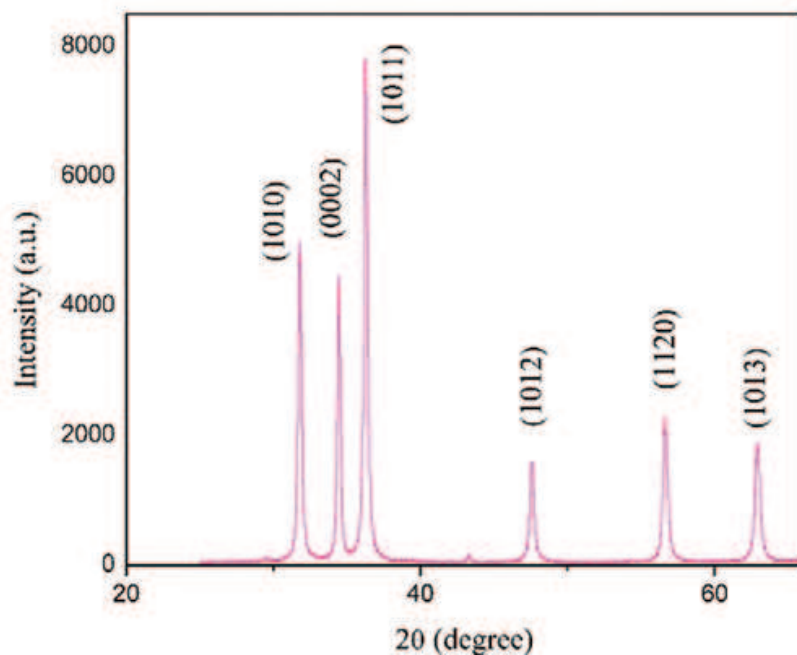**Table 5.** Ball-milling specification for preparing ZnO nanoparticles.

Figure 11. XRD pattern of zinc oxide powder obtained by reaction with water.

were slightly larger than those reported in corresponding JSPDS card number for bulk ZnO (a = 3.2498 Å and c = 5.2066 Å).

Zinc oxide particles obtained by this method are of two different morphologies: hexagonal flakes and rod structure. Depicted in **Figure 12a** is SEM of densely stacked hexagonal flakes. The average size of flakes is 200 nm. **Figure 12b** shows the TEM image of the second morphology (rod structure) with average length and diameter of 100 and 20 nm, respectively. Selected-Area Electron Diffraction (SAED) pattern of the powder is depicted just below **Figure 12b**. It can be indexed as hexagonal Wurtzite-structural ZnO, which is consistent with the analysis of XRD. The specific surface area of the powder obtained in our experiment was 18.25 m^2/g. It is, of course, a function of ball-milling specifications.

Theoretical explanation of the mechanism of synthesizing zinc oxide by abovementioned method may be represented as following: zinc atoms react with water to give zinc oxide. However, this happens only for the outermost atoms of a zinc particle because the zinc oxide (or zinc hydroxide) crust prevents water from diffusing into the particle, and consequently, inner atoms do not react with water. If the powder is milled together with brittle particles
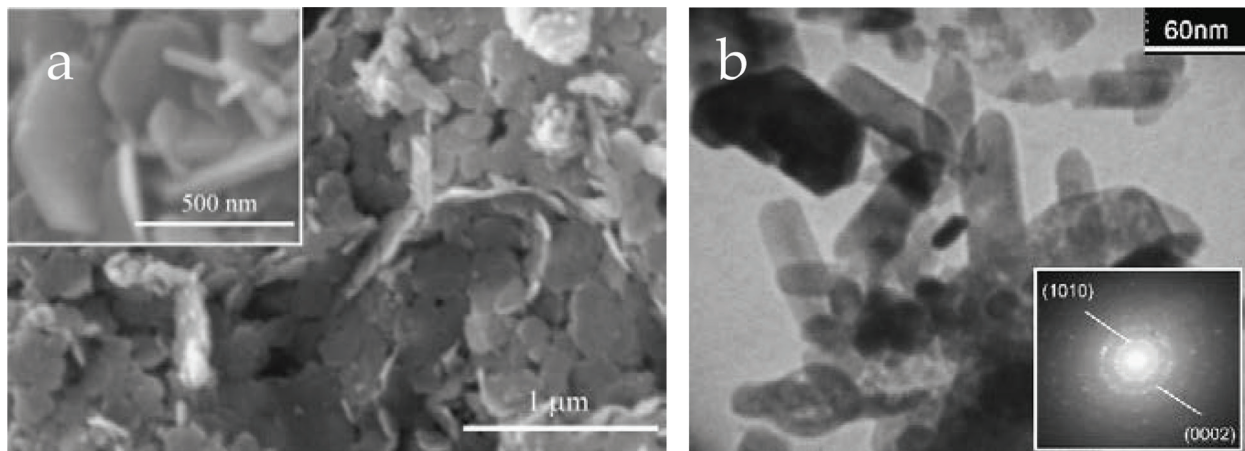
Figure 12. (a) SEM image of ZnO powder and (b) TEM image of ZnO powder and its corresponding SAED pattern (inset).

of salt, the oxide layer initially formed on the Zn particles is destroyed and newly produced surfaces are immediately covered by salt particles. Therefore, the activity of powder does not decrease after long-term storage in the air. When the powder is submerged by water, the salt is washed away, and zinc atoms are exposed to water and react with it:

$$Zn + 2H_2O \rightarrow Zn(OH)_2 + H_2 \tag{2}$$

Due to direct contact of zinc atoms with warm water, kinetics of reaction is rapid. Thus, a considerable amount of hydrogen is generated in each particle and in its way out, it burst open the zinc oxide or zinc hydroxide crust, exposing more fresh zinc to water. Hence, provided that zinc particles are small enough, all the contents of zinc is converted to zinc oxide. Zinc hydroxide contents are also hydrated to give zinc oxide as indicated by following reaction:

$$Zn(OH)_2 \rightarrow ZnO + H_2O \tag{3}$$

Unlike reaction (2) that is exothermic, reaction (3) is endothermic [57]. Warm water provides required energy for the reaction. The zinc oxide particles obtained from reaction (3) serve as seeds for agglomeration leading to a planar hexagonal nuclei. Zinc oxide lattice (as suggested by crystal habit of wurtzite ZnO) is composed of tetrahedrons with a zinc atom at the center and four oxygen atoms at the vertices. Hence, the (0001) planes in the hexagonal sheet is zinc-rich while the opposite plane (i.e., $(000\bar{1})(000\bar{1})$) is oxygen-rich. Li et al. put a rule forward according which the fastest growth rate of zinc oxide happens along $[000\bar{1}]$ direction and the rate of growth along other directions obey the following relation [58]:

$$V[0001] > V[01\bar{1}\bar{1}] > V[01\bar{1}0] > V[01\bar{1}1] > V[000\bar{1}] \tag{4}$$

Based on their rule, <0001> direction is the most preferable direction for zinc oxide nanoparticles to grow or aggregate. Two-dimensional hexagonal structures imply that the growth is hindered in this direction and the crystals grow along <$10\bar{1}010\bar{1}0$> direction. This may be due to

resident Cl^- ions. Cl^- ions are adsorbed preferentially on the positive polar face of the (0001) surface, which limits the axis growth along the <0001> direction and accelerates the radial growth [59]. Thus, the morphology of synthesized particles can be controlled by manipulating the concentration of the ions in the media.

5. Conclusion

A simple method for preparing nanoparticles of ductile metals by means of ball milling was proposed based on the experiments reported by others and experiments conducted by the authors. The essential point of the method is using a brittle material as nanochopper during the ball milling. The method showed to be very useful and leads to good results. In all the cases represented in this chapter, salt was used as the brittle material (the nanochopper). However, other ductile materials may be employed according to the nature of the experiment and ultimate purpose of preparing the nanoparticles.

Author details

Babak Alinejad* and Yazdan Zare

*Address all correspondence to: 16nd114n@vc.ibaraki.ac.jp

Ibaraki University, Hitachi, Japan

References

[1] Alinejad B, Mahmoodi A. Synthesis of graphene nanoflakes by grinding natural graphite together with NaCl in a planetary ball mill. Functional Materials Letters. 2017;**10**(04):1750047. DOI: 10.1142/S1793604717500473

[2] Alinejad B, Mahmoodi K. A novel method for generating hydrogen by hydrolysis of highly activated aluminum nanoparticles in pure water. International Journal of Hydrogen Energy. 2009;**34**(19):7934-7938. DOI: 10.1016/j.ijhydene.2009.07.028

[3] Mahmoodi K, Alinejad B. Enhancement of hydrogen generation rate in reaction of aluminum with water. International Journal of Hydrogen Energy. 2010;**35**(11):5227-5232. DOI: 10.1016/j.ijhydene.2010.03.016

[4] Mahmoodi K, Alinejad B. Fast and facile synthesis of boehmite nanofibers, powder technology. 2010;**199**(3):289-292. DOI: 10.1016/j.powtec.2010.01.019

[5] Alinejad B, Mahmoodi K, Ahmadi K. A new route to mass production of metal hydroxide/oxide hydroxide nanoparticles. Materials Chemistry and Physics. 2009;**118**(2-3):473-476. DOI: 10.1016/j.matchemphys.2009.08.020

[6] Suryanarayana C. Mechanical alloying and milling. Marcel Dekker. 2004:87-89. DOI: 10.1080/10426910701416344

[7] Geim AK, Novoselov KS. The rise of graphene. Nature Materials. 2007;**6**:183. DOI: 10.1038/nmat1849

[8] Geim AK, MacDonald AH. Graphene: Exploring carbon flatland. Physics Today. 2007;**60**(8):35. DOI: 10.1063/1.2774096

[9] Novoselov KS, Geim AK, Morozov SV, Jiang D, Zhang Y, Dubonos SV, Grigorieva IV, Firsov AA. Electric field effect in atomically thin carbon films. Science. 2004;**306**(5696):666-669. DOI: 10.1126/science.1102896

[10] Wang F, Zhang Y, Tian C, Girit C, Zettl A, Crommie M, Ron Shen Y. Gate-variable optical transitions in graphene. Science. 2008;**320**(5873):206-209. DOI: 10.1126/science.1152793

[11] Lee C, Wei X, Kysar JW, Hone J. Measurement of the elastic properties and intrinsic strength of monolayer graphene. Science. 2008;**321**(5887):385-388. DOI: 10.1126/science.1157996

[12] Robinson JT, Keith Perkins F, Snow ES, Wei Z, Sheehan PE. Reduced graphene oxide molecular sensors. Nano Letters. 2008;**8**(10):3137-3140. DOI: 10.1021/nl8013007

[13] Blake P, Brimicombe PD, Nair RR, Booth TJ, Jiang D, Schedin F, Ponomarenko LA, Morozov SV, Gleeson HF, Hill EW, Geim AK, Novoselov KS. Graphene-based liquid crystal device. Nano Letters. 2008;**8**(6):1704-1708. DOI: 10.1021/nl080649i

[14] Ji Z, Shen X, Song Y, Zho G. In situ synthesis of graphene/cobalt nanocomposites and their magnetic properties. Materials Science and Engineering B. 2011;**176**(9):711-715. DOI: 10.1016/j.mseb.2011.02.026

[15] Reina A, Jia X, Ho J, Nezich D, Son H, Bulovic V, Dresselhaus MS, Kong J. Large area, few-layer graphene films on arbitrary substrates by chemical vapor deposition. Nano Letters. 2009;**9**(1):30-35. DOI: 10.1021/nl801827v

[16] Sutter PW, Flege J, Sutter EA. Epitaxial graphene on ruthenium. Nature Materials. 2008;**7**:406-411. DOI: 10.1038/nmat2166

[17] Berger C, Song Z, Li T, Li X, Ogbazghi AY, Feng R, Dai Z, Marchenkov AN, Conrad EH, First PN, de Heer WA. Ultrathin epitaxial graphite: 2D electron gas properties and a route toward graphene-based nanoelectronics. The Journal of Physical Chemistry B. 2004;**108**(52):19912-19916. DOI: 10.1021/jp040650f

[18] Park S, Ruoff RS. Chemical methods for the production of graphenes. Nature Nanotechnology. 2009;**4**:217-224. DOI: 10.1038/nnano.2009.58

[19] Kotov NA, Dékány I, Fendler JH. Ultrathin graphite oxide–polyelectrolyte composites prepared by self-assembly: Transition between conductive and non-conductive states. Advanced Materials. 1996;**8**:637-641. DOI: 10.1002/adma.19960080806

[20] Chandra S, Sahu S, Pramanik P. A novel synthesis of graphene by dichromate oxidation. Materials Science and Engineering B. 2010;**167**(3):133-136. ISSN:0921-5107. DOI: 10.1016/j.mseb.2010.01.029

[21] Zhamu A, Zhang B Z. Environmentally benign graphite intercalation compound composition for exfoliated graphite, flexible graphite, and nano-scaled graphene platelets. US patent claim 20090028778; 2009

[22] Geng Y, Wang SJ, Kim J. Preparation of graphite nanoplatelets and graphene sheets. Journal of Colloid and Interface Science. 2009;**336**(2):592-598. ISSN 0021-9797. DOI: 10.1016/j.jcis.2009.04.005

[23] Arsat R, Breedon M, Shafiei M, Spizziri PG, Gilje S, Kaner RB, Kalantar-zadeh K, Wlodarski W. Graphene-like nano-sheets for surface acoustic wave gas sensor applications. Chemical Physics Letters. 2009;**467**(4-6):344-347. ISSN 0009-2614. DOI: 10.1016/j.cplett.2008.11.039

[24] Drzal LT, Fukushima H. Graphite nanoplatelets as reinforcements for polymers. Polymer Preprints (American Chemical Society, Division of Polymer Chemistry). 2001;**42**(2):42-43

[25] Welham NJ, Berbenni V, Chapman PG. Effect of extended ball milling on graphite. Journal of Alloys and Compounds. 2003;**349**(1-2):255-263. ISSN:0925-8388

[26] Wakayama H, Mizuno J, Fukushima Y, Nagano K, Fukunaga T, Mizutani U. Structural defects in mechanically ground graphite. Carbon. 1999;**37**(6):947-952. ISSN:0008-6223

[27] Pierard N, Fonseca A, Colomer JF, Bossuot C, Benoit JM, Van Tendeloo G, Pirard JP, Nagy JB. Ball milling effect on the structure of single-wall carbon nanotubes. Carbon. 2004;**42**(8-9):1691-1697. ISSN:0008-6223. DOI: 10.1016/j.carbon.2004.02.031

[28] Knieke C, Berger A, Voigt M, Klupp Taylor RN, Röhrl J, Peukert W. Scalable production of graphene sheets by mechanical delamination. Carbon. 2010;**48**(11):3196-3204. ISSN:0008-6223. DOI: 10.1016/j.carbon.2010.05.003

[29] Sridhar V, Jeon J, Oh I. Synthesis of graphene nano-sheets using eco-friendly chemicals and microwave radiation. Carbon. 2010;**48**(10):2953-2957. ISSN:0008-6223. DOI: 10.1016/j.carbon.2010.04.034

[30] Sarathi R, Sindhu TK, Chakravarthy SR. Generation of nano aluminium powder through wire explosion process and its characterization. Materials Characterization. 2007;**58**(2):148-155. DOI: 10.1016/j.matchar.2006.04.014

[31] Meda L, Marra G, Galfetti L, Severini F, De Luca L. Nano-aluminum as energetic material for rocket propellants. Materials Science and Engineering C. 2007;**27**:1393-1396. DOI: 10.1016/j.msec.2006.09.030

[32] El S, Barberoglou M, Fotakis C, Viau G, Garcia C, Shafeev GA. Generation of Al nanoparticles via ablation of bulk Al in liquids with short laser pulses. Optics Express. 2009;**17**(15):12650-12659. DOI: 10.1364/OE.17.012650

[33] Kapdan IK, Kargi F, Oztekin R, Argun H. Bio-hydrogen production from acid hydro-lyzed wheat starch by photo-fermentation using different Rhodobacter sp. International Journal of Hydrogen Energy. 2009;**34**:2201-2207. DOI: 10.1016/j.ijhydene.2009.01.017

[34] de Souza RF, Padilha JC, Gonçalves RS, de Souza MO, Berthelot JR. Electrochemical hydrogen production from water electrolysis using ionic liquid as electrolytes: Towards the best device. Journal of Power Sources. 2007;**164**:792-798. DOI: 10.1016/j.jpowsour. 2006.11.049

[35] Kojima Y, Suzuki K, Fukumoto K, Sasaki M, Yamamoto T, Kawai Y, Hayashi H. Hydrogen generation using sodium borohydride solution and metal catalyst coated on metal oxide. International Journal of Hydrogen Energy. 2002;**27**:1029-1034. DOI: 10.1016/S0360-3199(02)00014-9

[36] Kotay SM, Das D. Biohydrogen as a renewable energy resource—Prospects and poten-tials. International Journal of Hydrogen Energy. 2008;**33**(1):258-263. DOI: 10.1016/j.ijhydene.2007.07.031

[37] U.S. Department of Energy. Office of fossil energy—Hydrogen Program Plan: Hydrogen from Natural Gas and Coal: the Road to a Sustainable Energy Future. Available from: https://www.netl.doe.gov/File%20Library/Research/Coal/ccbtl/fehydrogenplan2003.pdf [Accessed March 05, 2018]

[38] Tzimas E, Filiou C, Peteves SD, Veyret J B. Hydrogen storage: State of the art and future perspective, European Commission, Directorate General Joint Research Centre, Institute for Energy, Petten, the Netherlands. Available from: https://pdfs.semanticscholar.org/1fc0/398a56d147790df6b8af9aab677e1c04eeb6.pdf [Accessed: March 05, 2018]

[39] Kravchenko OV, Semenenko KN, Bulychev BM, Kalmykov KB. Activation of aluminum metal and its reaction with water. Journal of Alloys and Compounds. 2005;**397**:58-62. DOI: 10.1016/j.jallcom.2004.11.065

[40] Hiraki T, Takeuchi M, Hisa M, Akiyama T. Hydrogen production from waste aluminum at different temperatures with LCA. Materials Transactions. 2005;**46**(5):1052-1057. DOI: 10.2320/matertrans.46.1052

[41] Andersen ER, Andersen EJ. Method for producing hydrogen. US Patent 6506360; 2003

[42] Martínez SS, Sanchez LA, Alvarez Gallegos AA, Sebastian PJ. Coupling a PEM fuel cell and the hydrogen generation from aluminum waste cans. The International Journal of Hydrogen Energy. 2007;**32**:3159-3162. DOI: 10.1016/j.ijhydene.2006.03.015

[43] Parmuzina AV, Kravchenko OV. Activation of aluminum metal to evolve hydrogen from water. International Journal of Hydrogen Energy. 2008;**33**:3073-3076

[44] Ilyin AP, Gromov AA, Reshetov AA, Tihonov DV, Yablunowsky GV. Reactionary abil-ity of aluminum ultrafine powders in various oxidation processes. In: The 4th Russian-Korean International Symposium on Science Technology KORUS Proceedings. Vol. 3; 2000. pp. 299-304

[45] Ivanov VG, Safronov MN, Gavrilyuk OV. Macrokinetics of oxidation of ultradisperse aluminum by water in the liquid phase. Combustion, Explosion, and Shock Waves. 2001;**37**(2):173-177

[46] Fan MQ, Xu F, Sun LX, Zhao JN, Jiang T, Li WX. Hydrolysis of ball milling Al–Bi–hydride and Al–Bi–salt mixture for hydrogen generation. Journal of Alloys and Compounds. 2008;**460**:125-129

[47] Fan MQ, Xu F, Sun LX. Studies on hydrogen generation characteristics of hydrolysis of the ball milling Al-based materials in pure water. International Journal of Hydrogen Energy. 2007;**32**:2809-2815

[48] Liu CH, Zapien JA, Yao Y, Meng XM, Lee CS, Fan SS, Lifshitz Y, Lee ST. High-density, ordered ultraviolet light-emitting ZnO nanowire arrays. Advanced Materials. 2003; **15**:838-841. DOI: 10.1002/adma.200304430

[49] Musić S, Dragčević Đ, Popović S, Ivanda M. Precipitation of ZnO particles and their properties. Materials Letters. 2005;**59**:2388-2393. DOI: 10.1016/j.matlet.2005.02.084

[50] Wang ZL. Nanostructures of zinc oxide. Materials Today. 2004;**7**(6):26-33. ISSN:1369-7021. DOI: 10.1016/S1369-7021(04)00286-X

[51] Kumar S, Kim YJ, Koo BH, Gautam S, Chae KH, Kumar R, Lee CG. Room temperature ferromagnetism in chemically synthesized ZnO rods. Materials Letters. 2009;**63**(2):194-196. ISSN:0167-577X. DOI: 10.1016/j.matlet.2008.09.057

[52] Ouyang W, Zhu J. Catalyst-free synthesis of macro-scale ZnO nanonail arrays on Si substrate by simple physical vapor deposition. Materials Letters. 2008;**62**(17-18):2557-2560. ISSN:0167-577X. DOI: 10.1016/j.matlet.2007.12.051

[53] Nagase M, Suhara M, Miyamoto Y, Furuya K. Peak width analysis of current–voltage characteristics of triple-barrier resonant tunneling diodes. Japanese Journal of Applied Physics. 2000;**39**:3314-3318 (Part 1, Number 6A)

[54] Lepot N, Van Bael MK, Van den Rul H, D'Haen J, Peeters R, Franco D, Mullens J. Synthesis of ZnO nanorods from aqueous solution. Materials Letters. 2007;**61**(13):2624-2627. ISSN:0167-577X. DOI: 10.1016/j.matlet.2006.10.025

[55] Chenglin Y, Dongfeng X. Solution growth of nano- to microscopic ZnO on Zn. Journal of Crystal Growth. 2008;**310**(7-8):1836-1840. ISSN:0022-0248. DOI: 10.1016/j.jcrysgro.2007.10.060

[56] Nakamura R, Lee JG, Tokozakura D, Mori H, Nakajima H. Formation of hollow ZnO through low-temperature oxidation of Zn nanoparticles. Materials Letters. 2007;**61**(4-5): 1060-1063. DOI: 10.1016/j.matlet.2006.06.039

[57] Ge J, Tang B, Zhuo L, Shi Z. A rapid hydrothermal route to sisal-like 3D ZnO nanostructures via the assembly of CTA+ and $Zn(OH)_4^{2-}$: Growth mechanism and photoluminescence properties. Nanotechnology. 2006;**17**(5):1316-1323

[58] Li W, Shi E, Zhong W, Yin Z. Growth mechanism and growth habit of oxide crystals. Journal of Crystal Growth. 1999;**203**(1-2):186-196. DOI: 10.1016/S0022-0248(99)00076-7

[59] Xu L, Guo Y, Liao Q, Zhang J, Xu JD. Morphological control of ZnO nanostructures by electrodeposition. Physical Chemistry B. 2005;**109**:13519-13522. DOI: 10.1021/jp051007b